Ocean Dynamics (2003) 53: 146–165
DOI 10.1007/s10236-003-0029-8

Emil V. Stanev · Götz Flöser · Jörg-Olaf Wolff

First- and higher-order dynamical controls on water exchanges between tidal basins and the open ocean. A case study for the East Frisian Wadden Sea

Received: 24 October 2002 / Accepted: 7 March 2003

Abstract Observational data, high-resolution numerical modelling results and a simple analytical theory are combined in this paper to demonstrate the dependence of the volume transports through tidal inlets on topographical or morphological parameters of a Wadden Sea system. The area of interest covers the East Frisian Wadden Sea and consists of seven weakly connected tidal basins. The observations include time series of tidal gauge data and surface currents measured at a pile station in the backbarrier basin of the island Langeoog, as well as several ADCP transects in the Accumer Ee tidal inlet. The numerical simulations are based on the 3-D primitive equation General Estuarine Transport Model (GETM) with a horizontal resolution of 200 m and terrain following vertical coordinates. The model is forced at its open boundaries with sea-level data from an operational model for the German Bight (German Hydrographic Office). The simple theoretical concepts presented illustrate the effect of topography (hypsometry) in the tidal basins on the temporal variability of the exchange of water. This topographic control is effectuated through the bottom slope in the areas prone to drying and flooding. For our study area it takes about twice as long from slack water to maximum flood current than from slack water to maximum ebb current. The underlying physics of this signal modulation from a more or less harmonic forcing at the open-sea boundary and the quantification of the contributing physical processes are the major results of this paper. Estimates based simply on volume conservation are consistent with observations and results from numerical modelling, but they do not completely capture the actual non-linear tidal response. Our analysis shows that at least during part of the tidal cycle characteristic topographic parameters of the inlet/bay system have a major impact on the rate of exchange of waters between the Wadden Sea and the open ocean. This impact is especially strong during the transition between flood and ebb conditions. The possible morphodynamic responses are also addressed focusing on some common (''universal'') topographic features in seven tidal basins.

Keywords Wadden Sea · Hypsometry · Dynamics and morphodynamics · Water exchange · Numerical modelling · Observations · Reference states in near coastal (tidal) dynamics · Universal topography control

Responsible Editor: Hans Burchard

E. V. Stanev (✉) · J.-O. Wolff
Institute for Chemistry and Biology of the Sea (ICBM),
University of Oldenburg, Postfach 2503,
26111 Oldenburg, Germany
e-mail: e.stanev@icbm.de

G. Flöser
Institute for Coastal Research,
GKSS Research Centre, Geesthacht, Germany

1 Introduction

The exchange of water, including various dissolved substances or suspended material, between the open ocean and coastal areas has a pronounced impact on the entire oceanic system. This exchange is quite vigorous in some areas characterized by complex bathymetry, and sometimes controls the evolution of the bathymetry itself. One such region is the East Frisian Wadden Sea (see Fig. 1 for a general overview of the area of interest). The tidal range is ~ 3 m and, according to the classification of Hayes (1979), this region is exposed to upper mesotidal conditions. About 10^8 m^3 of water is transported four times a day through narrow tidal inlets connecting the North Sea with the backbarrier basins. The width of the inlets ranges from 1–3 km. The exact volume transport through the various inlets in the chain of islands in the East Frisian Wadden Sea is still unknown. Even more important is that the temporal variability of the water exchange between the tidal basins and the open ocean is not sufficiently understood. This problem is the focus of the present study.

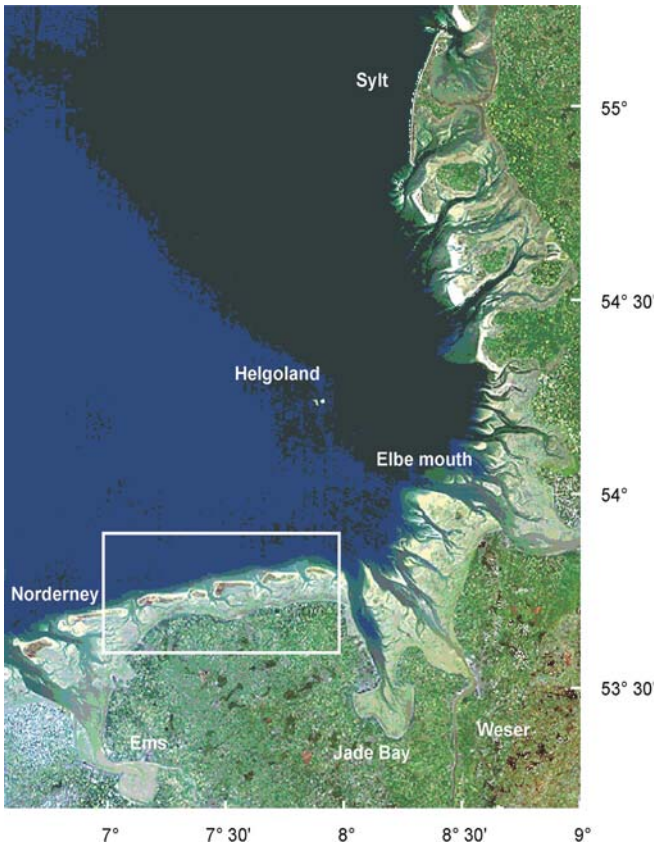

Fig. 1 The German Bight and the East Frisian Wadden Sea (*in the rectangle frame*). The yellow-grey colour gives approximately the areas of the tidal flats. (Landsat 5/TMAP, processed by GKSS)

The current uncertainties in quantitative estimates of the water exchange regime are based on an insufficient observational database as well as on an incomplete physical understanding of the system. One step towards improving the knowledge in this field was achieved after the Institute for Coastal Research, GKSS Research Centre, Geesthacht, Germany, initiated a long-lasting measuring programme (see Sect. 3 for more details). The second important step is due to numerical modelling, which gives an important complement to observations. Nowadays, it has become common practice in physical oceanography to use sufficiently validated models as tools to understand the details of the dynamics (e.g., by revealing details in variables which are not easily observed, or by allowing adequate sampling of the processes). Such a study has been carried out by Stanev et al. (2003, hereafter SWBBF) for the area of the East Frisian Wadden Sea, and the present work uses the model setup described there, as well as some of the simulated data.

The paper of SWBBF demonstrated that the circulation in the Wadden Sea is characterized by a large diversity of spatial patterns and a specific temporal variability. It became evident from this work that: (1) the oscillations of mean sea level in the tidal basins are not identical to those in the open ocean, and (2) the sea level in the tidal basins is characterized by large slopes. The latter creates a complicated structure of circulation precluding an accurate estimate of the water exchange with the open ocean from a limited number of sea-level observations only (e.g., gauges at coastal stations). In the present paper we objectively estimate the exchange of water between the tidal basins of the East Frisian Wadden Sea and the southern North Sea and the physical control on this exchange. There is always a challenge in physical oceanography to reveal the consistency between theoretical concepts, observations and numerical simulations. Sometimes the simulated results originating from sophisticated, but at the same time realistic, models are as complicated as the real data so that no clear understanding of the basic underlying processes can be easily obtained. Conceptual (idealized) models can thus help in increasing the harmony between theory and modelling. The present study gives one such example in the attempt to explain the dominating balances in the area of investigation with the help of a simple theory.

The paper is structured as follows: we first present some theoretical considerations on the water exchange and carry out a simple volumetric analysis based on the basin hypsometry. In Section 3 we discuss an estimate of water exchange based on the existing observations. In Section 4 we shortly describe the numerical model and the simulated data. The major focus of the paper, which is on the quantification of the role of physics, is addressed in Section 5, followed by conclusions.

2 Hypsometric approach to calculate the water exchange

2.1 The model area

The model area covers a good part of the East Frisian Wadden Sea (Fig. 1), and has a horizontal extension of about 65×17 km. The topographic map (Fig. 2) shows the typical morphological features usually observed in mesotidal basins: barrier islands, tidal inlets, tidal channels, tidal deltas and tidal flats. The grey colours of the near-coastal zone in Fig. 1 indicate areas which are prone to drying and flooding. Because a large part of this paper is devoted to the water exchanges of individual tidal basins with the open sea we first give a definition of ''individual basin''. Usually, the water sheds between the tidal channels are used to define the boundaries between the different basins. In order to make our definition consistent with what is accepted in the literature (e.g., Flemming and Davis 1994), to objectively find the water sheds and at the same time to remain close to the model formulations (see also Sect. 4), we define the horizontal extent of each basin by the waters coming in during an assumed constant (in space) flooding from its connecting inlet to the North Sea. Where the waters from two adjacent inlets meet, a watershed is defined and the boundary is fixed at that point. Thus the colour coding in Fig. 2b distinguishes seven tidal basins connected with the North Sea. The bound-

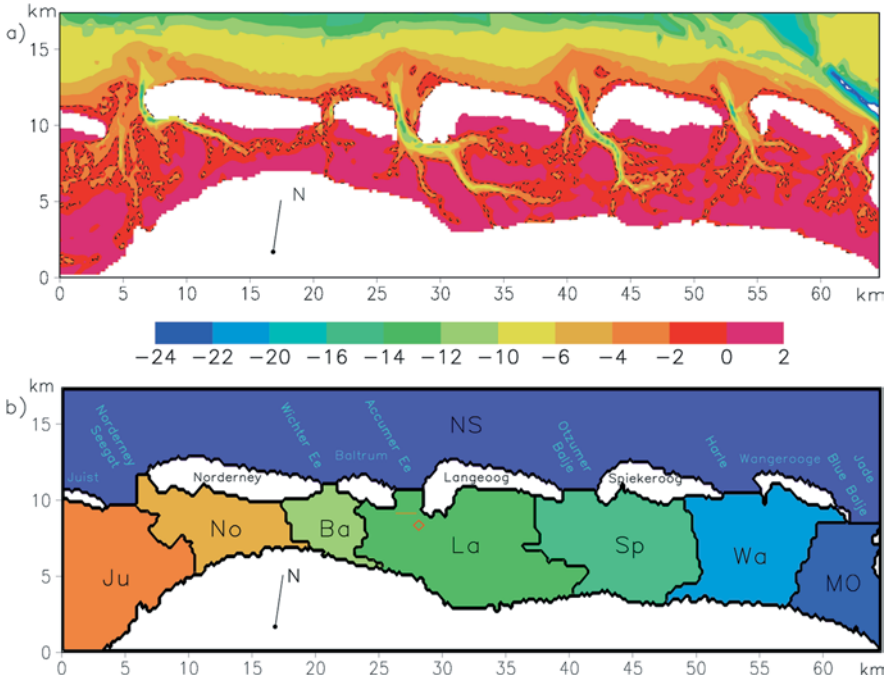

Fig. 2a, b Topography of East Frisian Wadden Sea. **a** The isobaths are represented as *negative numbers* (m) below the mean sea level. The *dashed isoline contours* indicate the depth 1.6 m below mean sea level, which is approximately equal to the amplitude of the spring tide. It thus specifies the areas which never fall dry during mean spring tide. The position of zero depth (in the figure the mean sea level) is calibrated in a way that the calculated changes in the volumes of individual basins are consistent with existing observational data (e.g., Ferk 1995). **b** Individual tidal basins. The *abbreviations* in the middle of each basin correspond to the names of the island behind which the corresponding tidal basin is located. The abbreviation *MO* stands for Minsener Oog (the small island on the eastern boundary of the model area identifying the easternmost tidal basin. *NS* denotes the part of the North Sea that is covered by our model grid. The *diamond symbol* gives the location where we analyze data from observations and simulations. The *short red line* in the Accumer Ee gives the approximate position where ADCP sections have been carried out and observations are used for model validation

aries between them roughly correspond to the boundaries of minimum water exchange specified in earlier studies (e.g., Flemming and Davis 1994). The bulk topographic characteristics of our model areas (mean volumes, basin areas, depths), presented in the study of SWBBF support some earlier estimates for the region (e.g., Ferk 1995) and can thus be considered as a realistic representation of the general topographic properties of this area. We demonstrated in our previous work that in this extremely shallow area the volume of the tidal prism $\Delta V = V_h - V_l$, i.e., the difference between the volumes for high (V_h) and low (V_l) waters, substantially exceeds V_l. In similar settings, the export and import of waters through the inlets may have different characteristic times, depending on the ratio between the maximum storage capacity of the basin and the water permanently stored in it. It is focal for the present paper that the tidal range in the deep part of the basin (this range is approximately equal to the tidal range north of the barrier islands) is larger than the depth below mean sea level measured over vast areas of the tidal basins. In order to illustrate this, we plot the dashed line in Fig. 2a, which corresponds to 1.6 m depth below mean sea level (this number approximates the amplitude of the tide in the model area). Obviously, the area prone to drying and flooding is larger than the remaining area of the tidal basins. This important topographic characteristic of the model area gives the major motivation to address here the response controlled by a basin area that changes with time.

2.2 Oscillations in almost enclosed bays with variable depth

The oscillations in a simple inlet-bay system can be described by the following system including momentum and continuity equations

$$\frac{\mathrm{d}u}{\mathrm{d}t} = \frac{g}{L_c}(\zeta_0 - \zeta) - \gamma|u|u \tag{1}$$

$$\frac{\mathrm{d}V}{\mathrm{d}t} = A_c u \ , \tag{2}$$

where u is the current velocity through the inlet, ζ is the sea-level elevation in the bay, ζ_0 the sea level in the open ocean,

$$V = \int_0^{\zeta} A_b(z)\mathrm{d}z \tag{3}$$

is the excess volume, g is the acceleration due to gravity, A_c and L_c the cross-sectional area of the inlet (or channel) and its length, respectively (the index c stands for channel), $A_b(z)$ the area of the bay (index b), z is directed upwards and γ is a friction parameter. Note that, unlike

in most analyses of the above system of equations, we assume here that the bay area A_b is a function of depth below the mean sea level $z = 0$. This important generalization was first addressed by Green (1992), who showed that including sloping side walls changes the behaviour of the Helmholtz oscillator and it becomes non-linear. Later, Maas (1997) extended the theory of Green towards the response of semi-enclosed bays driven by tidal oscillations. In the above system of equations we assume that the cross-sectional area of the inlet $A_c = \text{const}$. This is almost true if the inlet is deep and its sides almost vertical, and approximately corresponds to the shape of the inlets in our model area. Assuming $L_c = \text{const}$ is even less restrictive. On the whole, these two simplifications are much less restrictive than assuming $A_b = \text{const}$, which totally disagrees with the topographic features presented in the previous section, and its relaxation is the central point in the present study.

Equations (1) and (2) lead to a second-order differential equation for V (like a damped harmonic oscillator) forced by sea-surface oscillations in the open ocean ζ_0:

$$\frac{\mathrm{d}^2V}{\mathrm{d}t^2} + \gamma\frac{1}{A_c}\left|\frac{\mathrm{d}V}{\mathrm{d}t}\right|\frac{\mathrm{d}V}{\mathrm{d}t} + g\frac{A_c}{L_c}\zeta = g\frac{A_c}{L_c}\zeta_0 \quad . \tag{4}$$

In the case $A_b = \text{const}$ the solution of this equation is known as pumping or Helmholtz mode (Lighthill 1978) and describes the adjustment of the sea-level elevation in the bay to the external forcing. It gives a first-order estimate of the sea-level oscillation in real bays as well as the transport $\mathrm{d}V/\mathrm{d}t$ (see Eq. 2) through a real inlet.

Let us assume for simplicity that the bay area is a linear function of depth:

$$A_b = A_b^0\left(1 + \frac{z}{z_s}\right) \quad , \tag{5}$$

where A_b^0 and z_s are the basin area at mean sea level and a parameter controlling the steepness (index s) of the bottom, respectively. In the case of vertical side walls z_s is much larger than the tidal range, and $A_b \approx A_b^0$. In the case of tidal basins with large tidal flats z_s is small, i.e., the bottom slope in the tidal flat is small.

Equations (3) and (5) lead to the following non-linear relationship between sea level and excess volume:

$$V = A_b^0\left(1 + \frac{\zeta}{2z_s}\right)\zeta \quad . \tag{6}$$

In the case of vertical side walls ($\zeta \ll z_s$) the second term in the above equation vanishes and the system behaves like a classical Helmholtz oscillator.

The first solution of Eq. (6) gives for the sea level

$$\zeta = z_s\left(\sqrt{1 + \frac{2V}{V_0}} - 1\right) \quad , \tag{7}$$

where $V_0 = z_s A_b^0$. If $V \ll V_0$, and using the relation $(1+x)^{\frac{1}{2}} \approx 1 + \frac{1}{2}x$, we obtain from the above formula approximately

$$\zeta = \frac{z_s V}{V_0} = \frac{V}{A_b^0} \quad , \tag{8}$$

which is the relationship between sea level and volume in basins with vertical side walls. Proceeding in the same way with the second solution of Eq. (6) leads to the conclusion that this solution is unphysical.

The relevance of the above theory to the case in the East Frisian Wadden Sea is supported by the fact that around high water the flooded basin area is several times larger than around low water (see SWBBF). It becomes clear that if we substitute Eq. (7) in Eq. (4) and neglect the forcing and dissipation terms, the homogeneous equation

$$\frac{\mathrm{d}^2V}{\mathrm{d}t^2} + g\frac{A_c}{L_c}z_s\left(\sqrt{1 + \frac{2V}{V_0}} - 1\right) = 0 \tag{9}$$

will possess a non-linear behaviour (Green 1992; Maas 1997).

The physical explanation can be easily understood with the help of Fig. 3. In the deep basins without friction the classical Helmholtz mode is characterized by periodic exchange of bay and open-sea water and equal volumes of water transported through the inlets cause equal sea-level changes. In such a way a sinusoidal ζ_0 will force a sinusoidal response in the bay, that is assuming $V = A_b^0\zeta$ reduces Eqs. (1) and (2) to the following system of equations

$$\frac{\mathrm{d}u}{\mathrm{d}t} = \frac{g}{L_c}(\zeta_0 - \zeta) - \gamma|u|u, \tag{10}$$

$$\frac{\mathrm{d}\zeta}{\mathrm{d}t} = \frac{A_c}{A_b^0}u \quad . \tag{11}$$

From the above two equations we can derive the inviscid analogue of Eq. (4) assuming $\gamma = 0$:

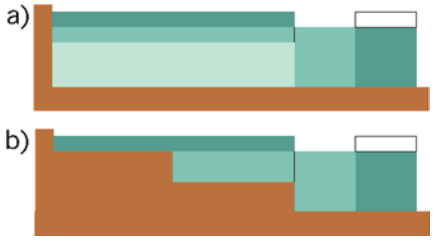

Fig. 3a, b Schematic representation of the bay-inlet system. **a** The bay has vertical side walls. **b** The area of the bay is a linear function of depth (see Maas 1997). The different colours focus on the fact that in **a** equal transport in the inlet (equal amount of subsequent entering packets of fluid) induces equal vertical displacement. The displacement in **b** decreases with the increase in the sea-level because the bay area is a function of the sea-level position. In this case more water through the inlet is needed to maintain equal sea-level rise, which indicates that the bay response is non-linear. The *contouring lines* above the second packet of fluid illustrate the fact that the packet can be displaced into the coastal area only if the water level is at least as high as the level in the bay. However, our simplifications do not consider this effect

$$\frac{d^2\zeta}{dt^2} + \omega_H^2 \zeta = \omega_H^2 \zeta_0 \quad , \tag{12}$$

where

$$\omega_H^2 = \frac{g}{L_c}\frac{A_c}{A_b^0} \tag{13}$$

is the pumping (Helmholtz) frequency. It is well known that equations of the type of Eq. (12) describe a linear response forced by ζ_0, for which it is essential that equal volumes of water entering the tidal basin cause equal sea-level response.

When the basin area increases with increasing the sea level, equal transports through the inlets produce different changes of sea level. At low water level the changes are larger than at high water level (Fig. 3b). This means that ebb conditions evolve faster than flood conditions. This conclusion supports the results of the study of Boon and Byrne (1981), the data analysis and results of one-dimensional numerical experiments by Friedrichs and Aubrey (1988), as well as the theoretical considerations of Friedrichs and Madsen (1992). It has been demonstrated by these authors that in estuarine systems where the storage area largely exceeds the area of channels, the tidal curves in the bays are steeper and the currents are faster during the ebb phase. The analysis of the simulations carried out by SWBBF demonstrated that this asymmetric response is also observed in the East Frisian Wadden Sea.

Here we go one step forward in the theoretical understanding of the non-linear response focusing on the temporal asymmetry of the transport. After linearizing Eq. (6) and taking the time derivative we find:

$$\frac{dV}{dt} = A_b^0\left(1 + \frac{\zeta}{2z_s}\right)\frac{d\zeta}{dt} \quad . \tag{14}$$

It is clear that for a given time rate of change $d\zeta/dt$ the resulting change of volume dV/dt will depend on: (1) whether the sea-level height is positive or negative, and (2) the ratio between the amplitude of the oscillations (a) and z_s. The first effect always leads to asymmetries associated with different times needed to establish maximum flood or ebb velocity. The second effect acts as an important non-linear selectivity and its amplitude dependence is typical for non-linear systems. By increasing $\frac{a}{2z_s}$, where a is the amplitude of oscillations, caused by a changing tidal range the transport curves will become steeper (see next section), the asymmetry in the transport will lead to an asymmetry in the sediment transport as well, the latter tending to increase z_s, thus changing the morphometry. From the point of view of morphodynamics z_s is no longer a key model parameter, but rather a function of the tidal range.

2.3 Tidal asymmetries due to topography. Water exchange based on hypsometric computations

There are two fundamental motivations to use the simple hypsometric analyses when addressing the exchange between tidal basins and the open sea (see also Boon and Byrne 1981). The first is that the Helmholtz mode is characterized by the absence of a spatial dependence of the sea-surface elevation. The second reason is that this is generally the most energetic mode, and the analysis focused on it should capture the main properties of the observed dynamics. The spatial homogeneity of the Helmholtz mode presents also an important consideration justifying the attempts presented further in the paper to develop simple schemes to infer the water exchange based on local sea-level observations.

The hypsometric curve gives the basin area A_b as a function of depth and Eq. (5) is one simple example of such a relationship. These curves and the corresponding basin volumes are presented in Fig. 4 for the seven tidal basins identified in Fig. 2. The computations are done in the interval 20 m below to 2 m above the mean sea level with 0.2 m vertical resolution. Obviously, these curves prove that: (1) the theoretical considerations given above are quite relevant to the East Frisian Wadden Sea, and

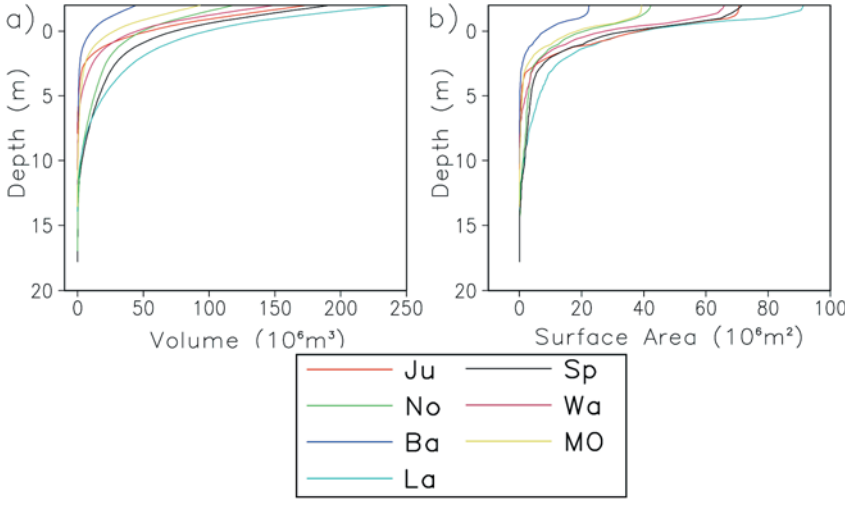

Fig. 4 Volumetric **a** and hypsometric **b** curves in the tidal basins. The topography in Fig. 2, which is actually the topography of the model, is used to compute the curves. The *explanation of the abbreviations* (names of tidal basins in the legend) is given in Fig. 2

(2) the major effects of "topography expansion" would occur in the upper 5 m (~5 m below the mean high water).

The generalized representation of the topography of individual basins using the hypsometric curves is even clearer in the corresponding normalized curves (Fig. 5). The normalization is done by dividing the basin volume (basin area) in Fig. 4 by the maximum basin volume (basin area) corresponding to the individual basins. After this normalization the curves converge, demonstrating that some "universal" profiles are valid for all basins. The latter could not be a simple coincidence, but rather demonstrates that the topography in the tidal basins is shaped by dynamics developing these universal morphometric characteristics. This is also an indication that even though the individual basins and their dynamics might seem different, the first-order morphodynamics controlling the major topographic properties appear quite similar.

It is noteworthy that Fig. 5b shows an almost linear increase of the basin area above the 2-m depth, i.e., in the intertidal flats, and that this increase is observed in all tidal basins. This "universal" rule (law) is probably associated with the regime of erosion and deposition tending to establish a bottom profile, which is coherent with the sea-level change. If we suppose that the rate of change of sea level between low and high water is constant, and that the sea-level oscillations exert the major dynamical control, then the horizontal propagation of the tidal wave should also have a constant time rate of change. The latter could happen if the basin area is a linearly increasing function of depth. In this context we want to recall that a discussion of the non-linear oscillator for hypsometric curves other than linear ones is provided by Doelman et al. (2002).

The inflection of the curves occurs at $\sim$ 3 m below mean sea level. Below this depth the almost vertical hypsometric curves indicate the presence of narrow and deep tidal channels (compared to the rest of the basins).

To illustrate the physical consequences of these particular profiles of hypsometric curves we first non-dimensionalize Eq. (6) introducing $\zeta' = \frac{\zeta}{a}$ and $V' = \frac{V}{V_0}$:

$$V' = \varepsilon\zeta' + \frac{\varepsilon^2}{2}\zeta'^2 \quad , \tag{15}$$

where $\varepsilon = \frac{a}{z_s}$.

Suppose that the sea level in the bay follows approximately the external forcing (we recall that the Helmholtz mode is characterized by the absence of a spatial dependence of sea-surface elevation), and that the latter is sinusoidal. Thus we assume that the "resistance" of the inlet is relatively small, and the transport adjusts to the external forcing in a way that the variability in the basin mean sea level almost repeats that of the ocean. We will come to this hypothesis later in the paper when analyzing the observations (measured forcing and response) and model simulations.

If $\zeta' = \sin(2\pi t/T) = \sin(\omega t)$, where T is the tidal period, the volume change, which is equal to the transport trough the inlet, is

$$\frac{\mathrm{d}V'}{\mathrm{d}t} = \varepsilon\omega\cos(\omega t) + \varepsilon^2\omega\frac{1}{2}\sin(2\omega t) \quad . \tag{16}$$

Equation (16) simply states that the non-linearity due to the sloping side walls generates harmonics in the transport with twice the frequency. This usual behaviour of non-linear systems is easily explained below, again using Fig. 3b. Before doing so we will first stress an important characteristic of coastal oscillations using the example of the Helmholtz oscillator. In the case of

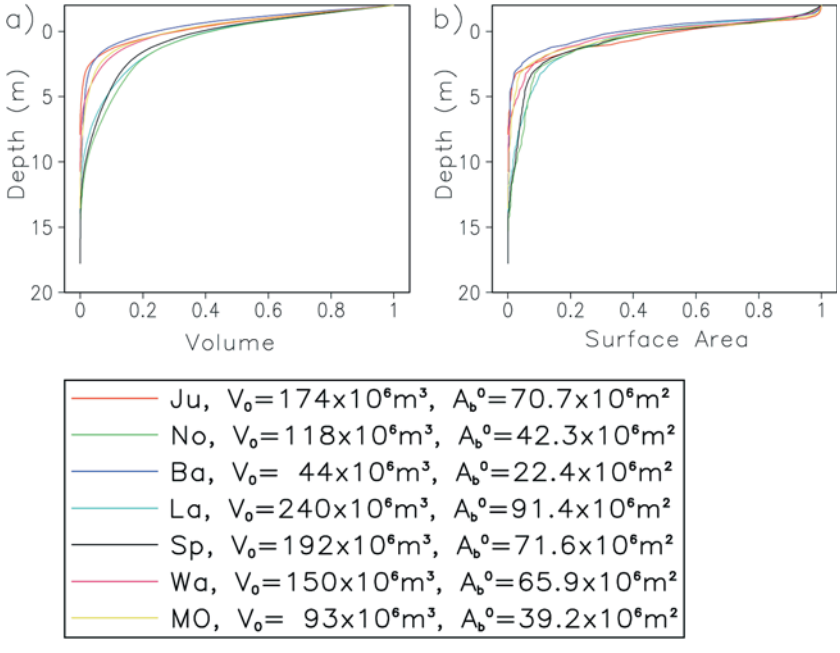

Fig. 5 Normalized volumetric **a** and hypsometric **b** curves in the tidal basins. The notations are given in the text. See also Fig. 2

vertical side walls Eq. (13) introduces an inverse proportionality between the Helmholtz frequency and the basin scale $B = \sqrt{A_b^0}$, that is $\omega_H \sim B^{-1}$. This is the analogue of the dispersion equation for shallow-water waves ($\omega \sim k$, where k is the wave number) of our specific physical system. Thus, shorter scales favour the generation of higher frequencies. We will replace for simplicity the linear hypsometry with a step-wise bottom, as this is the case in Fig. 3b. In this figure the extension of the deeper part is two times smaller than the extension of the shallow part (the latter is equal to the extension of the basin with vertical side walls in Fig. 3a). In this situation the new frequency generated by the topography change will be two times higher than that in the basin with vertical side walls.

The control of hypsometry becomes clear from Fig. 6a. The direction of velocity (positive towards the bay) reverses at the moment of high water ($t = 0.25T$). It takes $\frac{1}{6}T$ after $t = 0.25T$ for the ebb current to reach a maximum. At this time the sea level height has reached half of its maximum value. Because the emptying of the basin during this phase occurred at relatively high water the transport rapidly reached its highest value. After this time most of the volume of water stored in the bay has been exported, the water supply diminished and the ebb current started to decrease. It remained negative until the sea level started to rise again at $t = 0.75T$. Actually, almost zero water transport was established shortly before sea level reached a minimum. The inflection of the curve during the time of low water $t = 0.75T$ thus shows that there was no more water stored on the intertidal flats, and under sinking sea level the ebb currents almost ceased. The large storage capacity of the bay during periods of rising water results in much longer times needed for the flood current to reach maximum speeds ($t_{\text{flood}} = 2t_{\text{ebb}}$).

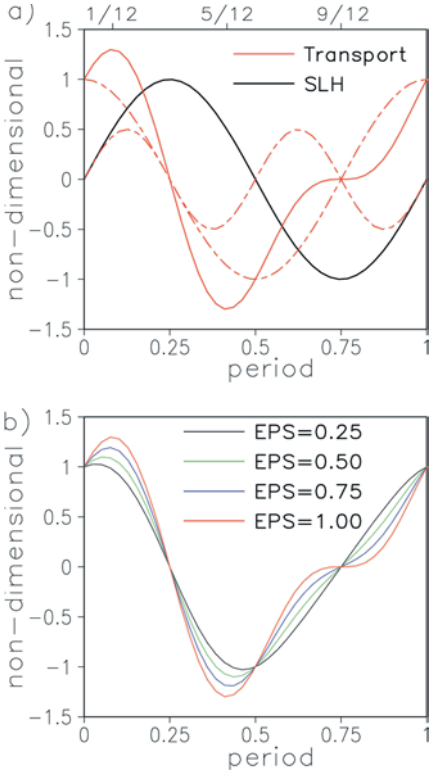

Fig. 6 **a** Sea-level height (*black line*) and inlet transport (positive when directed towards the bay, *the solid red line*). The *dashed lines* give the contribution of the two terms in Eq. (16). The computations are made for $\varepsilon = 1$ and the sea level and transports are normalized by a and ω, correspondingly. **b** Transports computed from Eq. (16) and normalized by $\varepsilon\omega$ for several values of ε

These relations describing the asymmetry in the response can be more easily understood from the following analysis. By differentiating Eq. (15) twice with respect to time, we obtain the conditions for extrema in the transport:

$$\frac{\mathrm{d}^2\zeta'}{\mathrm{d}t^2}(1+\varepsilon\zeta') + \varepsilon\left(\frac{\mathrm{d}\zeta'}{\mathrm{d}t}\right)^2 = 0 \ . \tag{17}$$

Assuming again that $\zeta' = \sin(2\pi t/T)$ we obtain

$$2\varepsilon x^2 + x - \varepsilon = 0 \ , \tag{18}$$

where $x = \sin(2\pi t/T)$. For the case $\varepsilon = 1$ (Fig. 6a) the solutions of the above algebraic equation are $x_1 = -1$ and $x_2 = \frac{1}{2}$. The first solution results in $t = \frac{3}{4}T$. This is a point of inflection (or saddle point) in the solid red curve in Fig. 6a, where $1 + \zeta = 0$ and $\mathrm{d}\zeta/\mathrm{d}t = 0$ at the same time (double zero). The second solution $\sin(2\pi t/T) = 1/2$ gives two extrema: at $t = \frac{T}{12}$ and $t = \frac{5}{12}T$. The corresponding times can be identified from the labelling of the upper x axis of Fig. 6a.

Figure 6b demonstrates the role of the non-linearity in establishing the asymmetry of the tidal response. Here the transports computed from Eq. (16) have been normalized by $\varepsilon\omega$ to show the dependence of the temporal asymmetry of the transport on the parameter ε. In the strongly non-linear case (ε tending to 1) the time difference between ebb and flood increases. These times become almost equal if ε is small, i.e., $a \ll z_s$.

The application of the hypsometric approach when calculating the volume and transports through the real straits (Fig. 7) demonstrates the same characteristics as in the theoretical model (Fig. 6). The curves in Fig. 7a,b differ mainly in their amplitudes. The short-period oscillations in the transport curves result from the topographic noise. The phase difference between times when transports reach maxima in the individual basins gives an indication about the delay of the tidal signal controlled by topography. This control is effectuated through the slope of the hypsometric curves, which is different in the different tidal basins. The oscillations in the basin volume reach maximum relative amplitudes for the smallest basin of Baltrum, while in the large basins of Langeoog and Spiekeroog the amplitudes are smaller. This is consistent with the analysis of topography in SWBBF, from where it follows that this ratio between tidal range and mean depth of tidal basins reaches largest values in the basin of Baltrum.

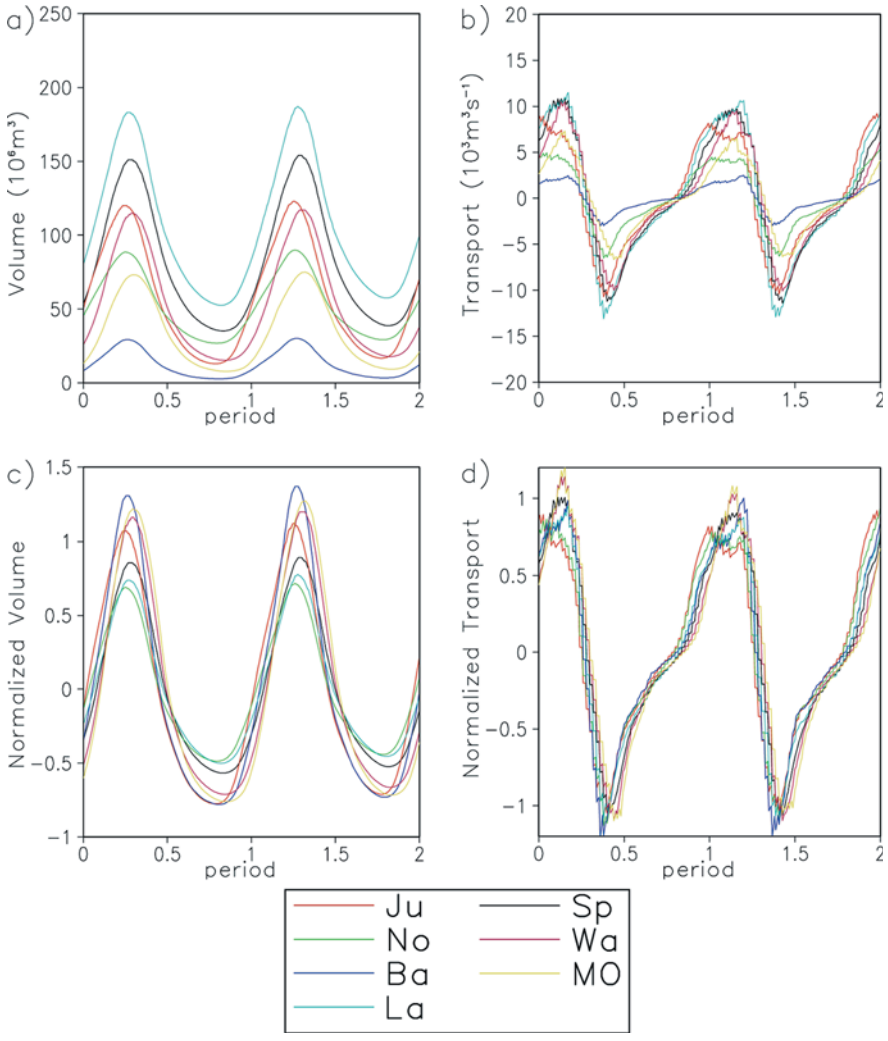

Fig. 7 Basin volume **a** and transport through the inlets **b** calculated from Eqs. (2), (3). The oscillations of sea level correspond to a typical spring tide. **c** and **d** The same results as **a** and **b** but normalized against the mean volumes and mean magnitude of the transports

2.4 The first-order physical control

The sensitivity of transports (estimated using the simple hypsometric concept) to the combined effect of sea level oscillations and variable topography is clearly demonstrated in the normalized transport curves (Fig. 7d). During most of the tidal cycle these curves lie in a tight envelope showing the universal topographic control on dynamics in the different basins. This result shows that when the transport is not extreme the basins behave physically almost identically. At extreme ebb, and particularly in flood, the transport curves differ, which indicates that these extreme events have the potential to substantially modify the topography.

The above results, which we obtained in a very simple way, seem to illustrate one important aspect of dynamical controls in the Wadden Sea, and motivate us to deepen the understanding about controls of different order. To go in this direction we have to identify first the most basic physics explaining the above results, that is, we will try to define the physical controls of different order and demonstrate how they are derived from the system of governing equations.

In the theory of waves the linearization is usually done with respect to a state of no motion. This zero-order state of the Helmholtz oscillator can be described with $\zeta = 0$, which is the mean sea level and $u = 0$. In the following we will derive the first-order physical control, as a model of the simplest balance governing the dynamics in tidal basins.

2.4.1 Diffusion of the tidal signal

The balance between pressure force and friction in shallow rivers was recognized by LeBlond (1978) as the dominating balance. Later, Friedrichs and Madsen (1992) investigated this balance in a number of shallow tidal embayments. These two studies succeeded in proving that the propagation of the tidal signal is more properly envisioned as a diffusion than as a wave-propagation phenomenon. To clarify the consequences of this balance we neglect the acceleration term in Eq. (10) and replace the friction term by a linear friction

$$\frac{g}{L_c}(\zeta_0 - \zeta) = \delta u \tag{19}$$

Equation (19) and Eq. (11) lead to the following equation:

$$\frac{\mathrm{d}\zeta}{\mathrm{d}t} = -\frac{\omega_H^2}{\delta}(\zeta - \zeta_0) \ , \tag{20}$$

which is an analogue to the diffusion equations studied by LeBlond (1978) and Friedrichs and Madsen (1992). In its simplest form (constant depth and linear friction) this equation has the form:

$$\frac{\partial\zeta}{\partial t} = K\frac{\partial^2\zeta}{\partial x^2} \ , \tag{21}$$

where $K = \frac{gh_c}{\delta}$ is the coefficient of diffusion which controls the propagation of tidal signal. Equation (20) describes the same process as Eq. (21) but for a tidal basin where ζ is assumed to be horizontal. Under frictional dynamical control morphodynamic equilibria are characterized by spatially uniform tides (Schuttelaars and de Swart 2000).

If the time scale in the right-hand side of Eq (21) is taken as $\frac{2\pi}{\omega}$, where ω is the forcing frequency (e.g., M2 tide), then the frictional (diffusion) length scale is

$$L_{fr} = \sqrt{\frac{2\pi g h_c}{\omega\delta}} \ . \tag{22}$$

The factor

$$T_{fr} = \frac{\delta}{\omega_H^2} \tag{23}$$

in Eq. (20) introduces the frictional time which controls the adjustment of the sea level in the bay to the forcing ζ_0.

The frictional length scale can also be expressed as

$$L_{fr} = L_g\sqrt{\frac{\omega}{2\pi\delta}} \ , \tag{24}$$

where

$$L_g = \sqrt{gh_c}T \tag{25}$$

is the frictionless tidal wavelength in water with constant depth h_c and tidal period T (see Schuttelaars and de Swart 2000).

The linear friction coefficient δ can be calculated as

$$\delta = \frac{gn^2}{h_c^{4/3}}|u_{\mathrm{mean}}| \tag{26}$$

(see also Eq. 10), where n is Mannings coefficient, for which we take the value of 0.027 $\mathrm{m}^{-1/3}\mathrm{s}$ (Bruun 1978). Thus for the M_2 tide ($\omega \sim 1.4 \times 10^{-4}$ s^{-1}), $|u_{\mathrm{mean}}| = 0.5$ ms^{-1} and $h_c = 10$ m the coefficient of linear friction $\delta = 1.7 \times 10^{-4}$ s^{-1}, $L_g \sim 45$ km and $L_{fr} = 0.26L_g$. It is clear from Eq. (24) that the ratio between forcing frequency ω and δ determines the relative strength of the frictional control (with increasing δ L_g decreases). Using Eq. (26) and the definition of the length scales (Eqs. 22, 25) we find $L_{fr} \sim \frac{h_c^{7/6}}{|u_{\mathrm{mean}}|^{1/2}}$ and $L_g \sim h_c^{1/2}$. The two different power lows demonstrate the different sensitivity of the two scales with respect to h_c, which is an illustration of the competing physical mechanisms in the different depth intervals. It follows from Eq. (24) and Eq. (26) that, depending on whether the tidal excursions $T|u_{\mathrm{mean}}|$ are smaller or larger than $h_c^{\frac{4}{3}}/gn^2$, the dynamics can change from inviscid to frictional control. The morphodynamic control should adjust accordingly. As seen in Fig. 2, the scales of tidal basins are ~10 km which is much smaller than L_g and agrees with the above estimates of L_{fr}.

If $\zeta_0 = a\sin\omega t$ the solution of Eq. (20) is

$$\zeta = \frac{a}{\sqrt{1+\omega T_{fr}}}\sin(\omega t - \theta) \ , \tag{27}$$

where $\theta = \arctan\omega T_{fr}$. It is clear now that the frictional response results in the fact that ζ follows ζ_0 in a simple aperiodic way. This type of response is meant in the following when we say that signal a follows signal b.

2.4.2 The sea level

In the theory of the Helmholtz oscillator we assume that the volume change is purely a result of the constant spatial sea-level variations. The solution of the homogeneous part of Eq. (12) gives periodic oscillations with frequency ω_H. Taking for the scales of the tidal basin the values which correspond to the tidal basin of Spiekeroog (see Sect. 5), we obtain $\omega_H \sim 1$ h.

The first assumption which we make here is that the oscillations in the tidal basin follow the oscillations in the open ocean. In the simplest case we can assume $\zeta \approx \zeta_0$. This assumption drastically constrains the spectrum of physical solutions in Eq. (1). In order to clarify this approximation we look again at Eq. (12). If we assume for the external forcing

$$\zeta_0 = a\cos\omega t \ , \tag{28}$$

where $\omega = \frac{2\pi}{T}$ and a are the forcing frequency and amplitude, respectively, we can find a particular solution of Eq. (12) in the form:

$$\zeta = a\alpha\cos\omega t \ , \tag{29}$$

where

$$\alpha = \frac{\omega_H^2}{\omega_H^2 - \omega^2} \tag{30}$$

is a distortion coefficient. In this case the velocity is:

$$u = -a\alpha\frac{A_b}{A_c}\sin\omega t \ . \tag{31}$$

We recall here that in systems without friction it is only the amplitude of the response which differs from the forcing signal, but not the phase.

A (formal) definition of the first-order physical control would assume that

$$\omega \ll \omega_H \ , \tag{32}$$

i.e., the pumping frequency is much larger than the frequency of the forcing signal, which results in $\alpha \approx 1$. In

this case the response of the sea level (Eq. 29) almost equals the forcing (Eq. 28).

If we replace the friction term in Eq. (1) by a linear friction

$$\frac{\mathrm{d}u}{\mathrm{d}t} = \frac{g}{L_c}(\zeta_0 - \zeta) - \delta u \ , \tag{33}$$

the frictional analogue of Eq. (12) is

$$\frac{\mathrm{d}^2\zeta}{\mathrm{d}t^2} + \delta\frac{\mathrm{d}\zeta}{\mathrm{d}t} + \omega_H^2\zeta = \omega_H^2\zeta_0 \ . \tag{34}$$

If we keep the forcing signal as defined by Eq. (28), the response will again be a simple harmonic function. The difference to the non-frictional case above would consist of adding a time lag, or phase difference, i.e.,

$$\theta = \frac{1}{\omega}\arctan\frac{\delta\omega}{\omega_H^2 - \omega^2} \ , \tag{35}$$

and a different distortion coefficient:

$$\alpha = \frac{\omega_H^4}{(\omega_H^2 - \omega^2)^2 + \delta^2\omega^2} \ . \tag{36}$$

Obviously, the distortion and phase lag are functions of the model parameters. We will demonstrate in the remainder of the paper that in the Wadden Sea the response closely follows the forcing. Thus, the specific balance is such that the friction is strong enough and suppresses oscillations associated with the pumping mode. In this case the momentum equation can be approximated by a balance between the pressure gradient force and friction. This can occur even when the friction coefficients are relatively small, thus eliminating significant distortions and lags in the response (see Sect. 5).

In summary, the first-order equations neglect all acceleration terms and any spatial variation in u and ζ. An additional linear friction term would not qualitatively change the main result, i.e., that the response is still mainly an amplitude-modulated function of the forcing with a small phase lag.

2.4.3 The conservation of mass

As seen in Fig. 7, in most of the tidal basins in the East Frisian Wadden Sea it takes more than twice the time to change from maximum ebb current to maximum flood current than vice versa. This asymmetry is central to an explanation of the transport processes in this area and fits well with the theoretical concepts developed in Section 2.3. The major assumption there is that the basin area is a linear function of depth. Invoking the continuity equation (Eq. 2) which, combined with the hypsometric relationship (Eq. 3) yields:

$$u = \frac{A_b(\zeta)}{A_c}\frac{d\zeta}{dt} \ . \tag{37}$$

This equation implies that the velocity is purely a result of the constant spatial sea-level variations modulated by the hypsometric curve.

In summary, the first-order physical processes imply that: (1) the momentum equation is reduced to $\zeta = \zeta_0$ or (in the more general case with a linear friction term) to a balance between pressure gradient force and friction, and (2) that the continuity equation is given by Eq. (37).

3 Observations

3.1 Description of observations

In the years 2000 to 2002, various hydrographic parameters were measured by GKSS in the German Wadden Sea using pile stations and ship campaigns. The pile stations were positioned in the tidal basin between the islands Langeoog and Baltrum (see Fig. 2 for the position of the pile station used in the present study). Among others the following oceanic parameters were measured: current speed and direction, turbidity, gauge level, wave height, conductivity and temperature. In addition, meteorological data have been recorded, i.e., air pressure and temperature, precipitation, wind speed and direction and solar irradiation. All data have been recorded as an average over a period of 10 min. During the ship campaigns, vertical current profiles were regularly measured using ADCP on transects across the Accumer Ee (see Fig. 2).

An independent source of data which is used to establish the relevance of the approaches developed in this study comes from the operational model of the German Federal Maritime and Hydrographic Agency (Bundesamt für Seeschiffahrt und Hydrographie, BSH). The BSH model is shortly described in Section 4.2. Below we will analyze the sea-level data measured and obtained from the BSH model.

3.2 Tidal response as correlation between sea level in the open sea and the backbarrier basins

One major focus in this paper is the distortion of the tidal signal in the backbarrier basins. The optimal data which could be desired when analyzing this distortion would be sea-level data measured north and south of the backbarrier islands. Unfortunately, most of the coastal tidal stations are located on the southern coasts. Therefore, for the North Sea area we use sea-level data from the BSH model, which were kindly provided by S. Dick. A detailed analysis of these data is presented in the study of SWBBF. It was found in this study (see also Fig. 8) that the sea level in the tidal basins is in phase with the sea level in the open ocean, which is close to sinusoidal. This important result justifies the definition of a first-order physical control in Section 2.4.

The small differences between the amplitudes in the two datasets seen in Fig. 8 indicate the degree of modulation of the tidal signal after passing through the inlets. Further analysis of the gauge level time series exemplifies the general characteristics of the region: the

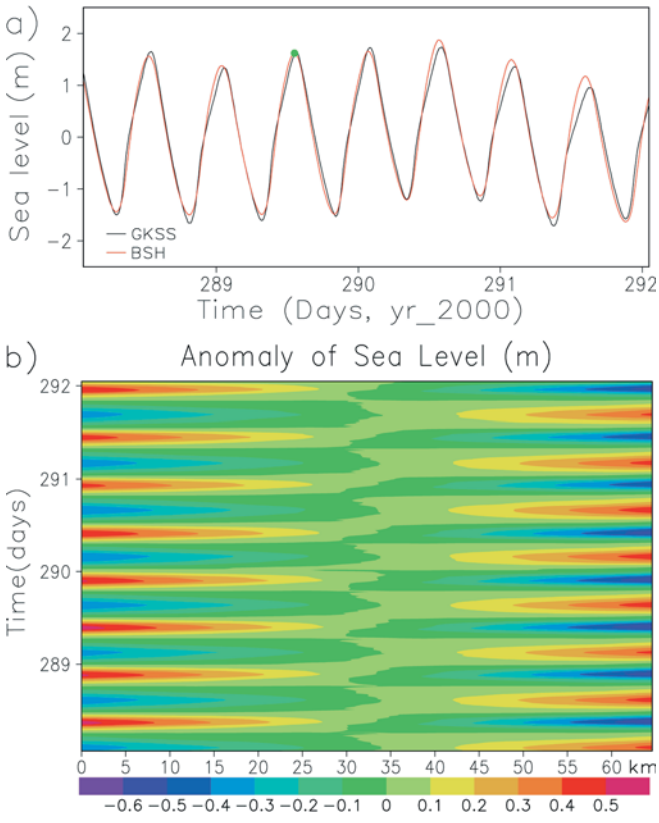

Fig. 8 **a** Variability of sea-surface elevation measured at the pile station (*black line*) during 14–18 October, 2000. The data from the operational model of BSH at the middle of the model open boundary are also plotted. The *green circle on the graph* marks approximately the time when high water occurs. We refer to this time marker in Section 4.3 when specifying the timing conventions used in the analysis of the simulated horizontal patterns. **b** Time–space diagram of the sea-level anomaly at the northern model boundary. Data from the operational model of BSH are used for the same period as in **a**

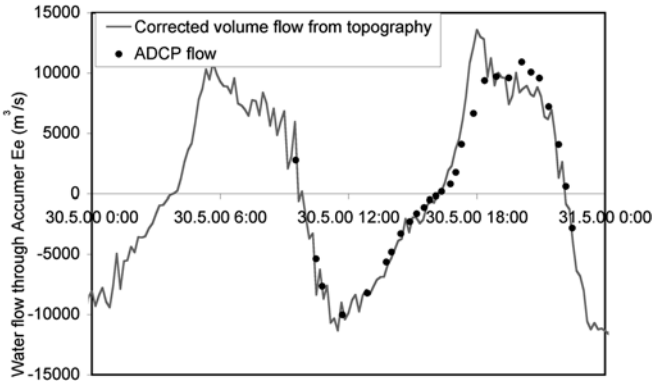

Fig. 9 Observed and reconstructed water transport through the Accumer Ee on May 30th, 2000. See text for the explanation of the computational procedure

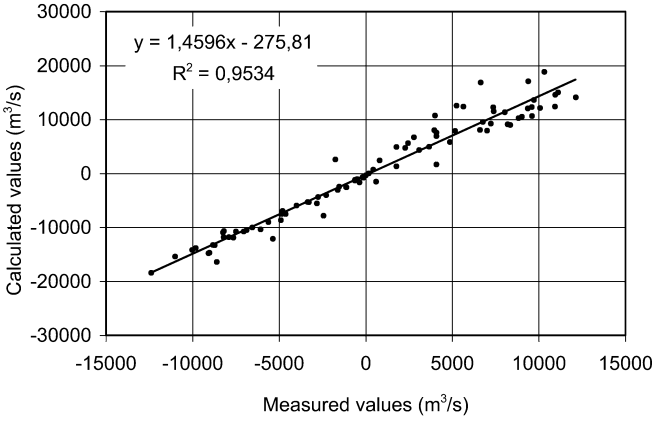

Fig. 10 Correlation between observed and calculated water transport (positive when directed towards the bay)

spring tidal range is 3.4 m, at neap tide it is about 1.8 m. The tidal signal arrives at the pile station near the tidal inlet Accumer Ee at 53 42.657 N 7 28.273 E 1 h earlier than at the two land stations at Dornumersiel and Bensersiel, where it arrives almost simultaneously.

3.3 Transports through the Accumer Ee

The ADCP transects across the main channel in the Langeoog basin gave a unique opportunity to test the general dynamical characteristics of the local tidal basins associated with the bulk export-import of water, as well as its temporal variability. The transport integrated over a flood/ebb period defines the volume of water accumulated in, or exported from, the tidal basins. This fundamental parameter, when compared against calculations based on the hypsometric approach, reveals whether a basin bathymetry is well resolved. This issue is of particular importance because the topography and the coastline are subject to variable sedimentation and because the quality of bathymetric data is often questionable. The shape of the transport curves, on the other hand, is indicative of the physical response of the backbarrier area.

The ADCP data represent important independent measurements in the context of the present study, because they enable us to calculate the volume flow for a full tidal cycle from the measured vertical profiles of the currents (see the dots in Fig. 9). The solid line in Fig. 9 was obtained as follows: for every gauge level measured at the pile station, a corresponding volume of the tidal basin was determined. For two subsequent measurements, the volume difference per time interval, i.e., a volume flow, was calculated. This volume flow was compared to the ADCP measurements carried out four times in 2000, each one covering at least one tidal cycle. The correlation between the two estimates reveals a clear linear relationship (see Fig. 10). The volumetric values were corrected with the linear correlation taken from Fig. 10 giving the solid line in Fig. 9. Using the gauge data from the pile station and the above described correlation, we can produce relatively accurate estimates for the volume flow through the Accumer Ee for the period May to November 2000.

The curve showing the water transport carries the same main characteristics of the tidal asymmetry which

we obtained with our simple theoretical model (Fig. 6), as well as with the volumetric computations presented in Section 2.3.

The agreement between the two independent estimates allows us to reconstruct the transports through any inlet in our model area using a very simple approach with sea-level data that are relatively easy to obtain. The small errors seen in Fig. 10 could be due to an overestimation of the size of the basin (the catchment area of the Accumer Ee) in the volumetric calculations, where the highest elevation between the basins is taken to be the watersheds. However, the "non-universal" response under extreme flood conditions (see Fig. 7d) is the more plausible candidate to explain the errors in Fig. 10.

It is noteworthy that the theoretical transport curves, those computed using the simple hypsometric approach, as well as those based on observations, contradict the view presented by Postma (1982) on the temporal asymmetries (see his Fig. 36). This view was based on the earlier work of the same author from 1954 (citation from Groen 1967) and suggests that the inward net flow of matter is a function of the time lag between currents and matter concentration. The paper of Groen (1967) can be used as a clear example of the problem. This author proposed a mechanism by which a net transport of suspended matter is generated in a purely alternating tidal current (zero residual transport and equal maximum currents at flood and ebb). The variability of the transport postulated by Groen (1967) suggests that

$$u \sim \sin(\omega t) + \frac{1}{2}\sin(2\omega t) \quad . \tag{38}$$

The comparison with (Eq. 16) for the case $\varepsilon = 1$ demonstrates that the phases of the higher harmonics in Eq. (38) and Eq. (16) differ by $\frac{\pi}{2}$ compared to the phase of the main oscillation (the M_2 tide). From the simple theory of Groen (1967) it follows that without the second term in Eq. (38), which is responsible for the asymmetry in water transport, no net transport of suspended mater would be possible (note that the net water transport is zero and the maximum flood and ebb velocities are equal). Following the theory of Groen (1967) and taking Eq. (16) for the variability of the transport would result in a net seaward sediment transport. Obviously, the "shorter-falling" asymmetry (in the terminology of Friedrichs and Madsen 1992), which is the dominating one in the tidal basins under consideration, cannot explain the landward net transport of suspended matter. Therefore further improvement in the understanding of dominating morphological balances is needed.

4 The model and some results of the simulations

4.1 Description of the model

Wadden Sea modelling goes back to Ridderinkhof and Zimmerman (1990) with simulations for the Western Dutch Wadden Sea, Hübner and Backhaus (1997), who carried out their simulations in part of the area of our interest and Dick and Schönfeld (1996) with simulations in the North Frisian Wadden Sea. Recent modelling efforts in the East Frisian Wadden Sea are discussed by SWBBF.

The present work is based on a relatively new model, the General Estuarine Transport Model (GETM) which, as has been demonstrated in our previous research, is quite appropriate for simulations of the circulation in the Wadden Sea. In the following we will briefly list some of the most important characteristics of the model, and in particular those which are of utmost importance when addressing the processes in our model area.

GETM is a 3-D primitive equation numerical model (Burchard and Bolding 2002) in which the momentum and continuity equations are supplemented by a pair of equations describing the time evolution of the turbulent kinetic energy k and its dissipation rate ε. The first application of this model to the area of our study is described by SWBBF and we refer to this paper for more details about the model presentation, its setup and forcing, as well as for results of simulations and model validations against observations.

A special aspect of GETM is its ability to adequately treat dynamics in deep inlets and channels, as well as on the intertidal flats, the latter falling dry during part of the tidal period. This is achieved by introducing a drying corrector, which reduces the influence of some terms in the momentum equations in situations of very thin fluid coverage on the intertidal flats. In the present simulations the areas where the water column is thinner than $D_{\min} = 2$ cm are considered dry. In the interval between $D_{\text{crit}} = 10$ cm and $D_{\min}$ the model physics are gradually switched towards friction domination, i.e., by reducing the effects of horizontal advection and Coriolis acceleration. For a water coverage greater than 10 cm the full physics are included.

In the horizontal we resolve the model domain with equidistant steps of 200 m and the horizontal matrix includes 324×88 grid points in the zonal and meridional direction, respectively. In order to reduce the number of land points in the model area we rotated the region bounded by the rectangular frame in Fig. 1 by $\sim 9^\circ$ (see the arrow pointing to the north in Fig. 2). In the vertical, the model uses terrain-following coordinates. The vertical discretization consists of ten equidistant layers extending from the bottom H to the sea surface ζ. Because ζ changes continuously during the model integration, the thickness of the water column D becomes a function of the sea level, i.e., the vertical discretization changes with time (keep in mind that the tidal range is comparable or exceeds the mean depth of tidal basins). In our model area the coarsest vertical resolution (in the deepest channels) is ~ 2 m. In the limiting case when the thickness of the water column approaches $D_{\min}$ the resolution is ~ 2 mm.

The simulations are carried out for the period between October 10 to 18, 2000; however, we will

discuss here only results from the period October 16 to 18, because this period is representative for the general conditions during spring tide. The aim of this paper is not an extensive model validation, neither do we want to address the assimilation of observations. Therefore we analyzed in Section 3 the observations during another typical spring tide period for which data were available in order to illustrate that the general properties of the transport curves obtained from theory and simple hypsometric computations match the observations qualitatively well. This decision was mainly motivated by our interest in: (1) extending the analysis of the model data of SWBBF, and (2) estimating the control of the model physics on the exchange through the inlets.

4.2 The model forcing

Sea-level data from the operational model of the BSH are used to provide boundary conditions for the model. The BSH model is a three-dimensional prognostic model (Dick and Sötje 1990; Dick et al. 2001) which operates in two versions: (1) a coarse-resolution model including the North Sea and Baltic Sea (grid size is 10 km), and (2) a high-resolution model of the German Bight where the horizontal resolution is 1.8 km. The boundary conditions at the open boundaries are formulated using tidal values calculated from the tidal constituents of 14 partial tides. The model predicts currents, water level, water temperature, salinity and ice coverage. At the sea surface the model is forced with meteorological and wave forecasts (wind, atmospheric pressure, wave characteristics, air temperature, specific humidity and clouds), which are provided by the German Weather Service.

The output of the BSH model incorporates one of the main elements of the regional circulation, that is, the coastal wave associated with the well-known amphidromy at $\sim (55.25°\mathrm{N}, 5.5°\mathrm{E})$. The tidal signal associated with the amphidromy travels through our model area of $\sim$60 km length in $\sim$50 min.

The model forcing is characterized by three major variabilities of the sea surface: (1) it undergoes vertical oscillations which appear almost instantaneously over the whole domain (Fig. 8a) because the scales of the domain are much smaller than the perimeter of the amphidromy in the North Sea, (2) it undergoes oscillations in an east–west direction (Fig. 8b) because the region is dominated by the slope of the sea surface during the different phases of the tide, and (3) the oscillations are subject to an east–west asymmetry, i.e., the tidal range tends to increase to the east (the contrasts between colours in the eastern part of Fig. 8b are greater than in the western part).

In the simulations presented here we did not include the effects of wind forcing, because we were so far only concerned with the effects of the tidal forcing on the water exchanges through the inlets.

4.3 Model performance

Because the present study is based on the same simulations as reported in the study of SWBBF, the results below are presented very briefly. We therefore concentrate on a discussion of the patterns of sea level and circulation. This focus is needed because we want to understand whether the assumption that the sea level is horizontal (this assumption is central in the hypsometric analysis) is justified from the model data, or whether higher-order dynamical controls are dominating.

The vertical motion of the sea level at the open boundary and its slope provide the major driving force for the model. The sea level in the tidal basins tends to adjust to the sea level in the NS area (see Fig. 2 for the nomenclature of tidal basins), as seen from the correlation between the sea level in the basin of Langeoog (Fig. 11a) and the forcing data (Fig. 8). The perturbations thus propagate along the channels because they provide the major pathway for the signal into the tidal basins.

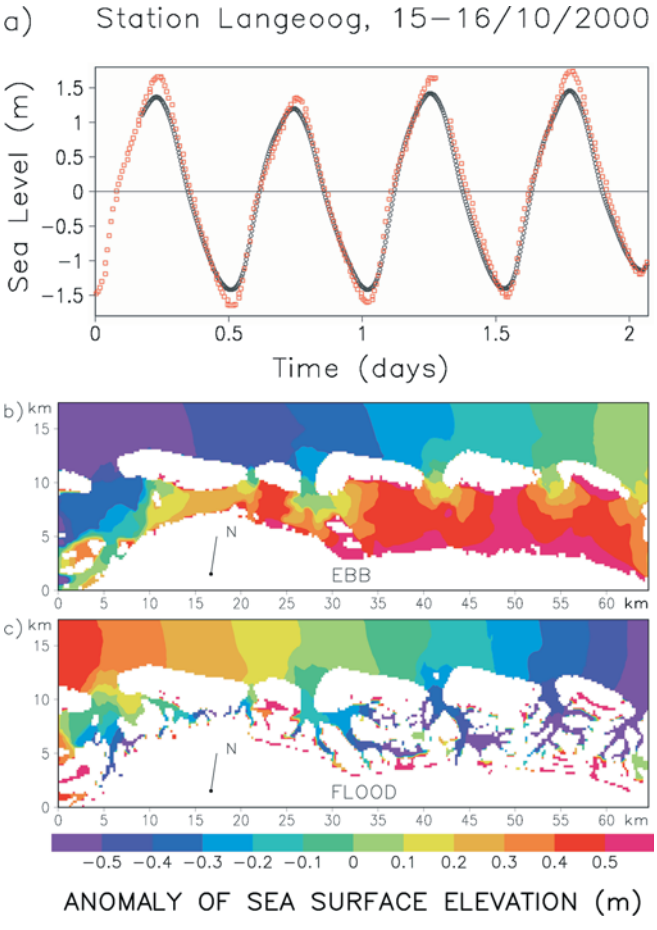

Fig. 11 **a** Temporal variability of the mean sea level in the backbarrier basin of Langeoog. The *red line* is based on observed data, the *black one* on simulations. **b** Horizontal patterns of the sea-surface height anomaly (deviation from the current area mean value) during ebb **b** and flood **c** phases of spring tidal cycle. The time corresponding to the first plot is a quarter tidal period to the right of the position of the green marker in Fig. 8a. The second plot is half a tidal period after the first one

The slope of the sea level north of the barrier islands is distinctly different during ebb and flood periods. During ebb, we have a falling sea level and the slope is from east to west. During flood the slope north of the islands is from west to east. The circulation in the model area is thus dominated by a westward transport during ebb and an eastward transport during flood (see Fig. 12). It has been demonstrated by SWBBF that, while the transport through the inlets is mainly governed by the amplitude of the tidal oscillations (see Eq. 11), the along-shore circulation, as well as the circulation in the intertidal areas, is governed by the spatial properties of the forcing signal. Our simulations are consistent with observations, e.g., Santamarina Cuneo and Flemming (2000), who demonstrated that maximum velocities in the Otzumer Balje exceed 1 ms^{-1}.

There is a pronounced similarity between the simulated dynamics in the individual inlets, particularly in the larger ones (from Harle to Accumer Ee), revealing that the dynamics in the individual basins obey the same physical balances.

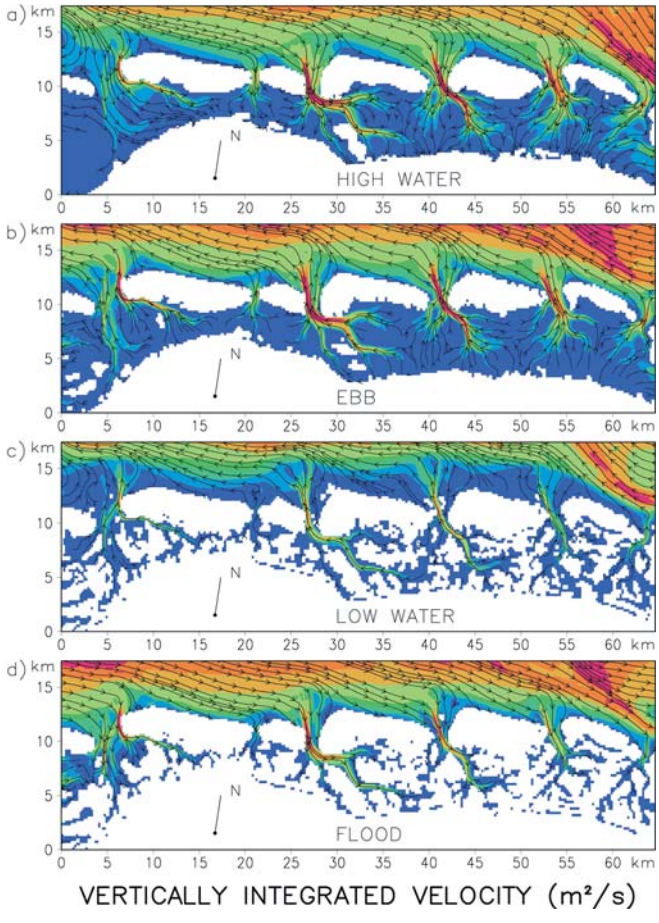

Fig. 12 Vertically integrated velocity during high water **a**, ebb **b**, low water **c** and flood **d** phases of the spring tidal cycle. The time of the first snapshot corresponds to the position of the green marker in Fig. 8a. The time interval between subsequent plots is a quarter tidal period

To assess the accuracy of our results presented in Section 3.3 it is important to mention that during ebb the difference between sea level in the Accumer Ee and on the intertidal flats south of the Islands Langeoog and Baltrum could reach ~ 0.5 m (see also Fig. 11 giving an idea about the spatial inhomogeneity). This result demonstrates that any simple calculation of the volumes based on local sea-level observations could be severely biased, i.e., that higher-order dynamical controls play a crucial role.

Looking at Fig. 13 we see that the first velocity maximum (in both observations simulations) corresponds to the flood and the second to the ebb (see also the bottom panel of Fig. 13). Most of the time the entire water column shows relatively strong vertical gradients and a high level of turbulence. Only during slack water (duration of ~ 1 h) do the vertical velocity gradients vanish and the level of turbulence diminish. It is noteworthy that the intensity of the transport in the Accumer Ee is slightly lower than in the Otzumer Balje (and so is the current shear in the vertical), which is supported by the comparison between the observations of Santamarina Cuneo and Flemming (2000) and our results, as well as by the comparison between Fig. 13 and Fig. 16 of SWBBF.

Consistent with our theoretical analysis (see Sect. 2), a longer time is needed in the model for the transition from maximum outflow to maximum inflow, i.e., it takes longer to decelerate the ebb flow and to accelerate the flood flow than it takes to decelerate the flood flow and accelerate the ebb flow, respectively. The maximum ebb velocity is observed shortly before the rate of sea level fall reaches its maximum at the open boundary (see also Fig. 6). However, the maximum flood velocity is delayed by $\sim$2 h with respect to the maximum rate of sea-level rise at the open boundary.

5 Estimating low- and higher-order dynamical controls

Below we present the results from two numerical experiments. Both are driven by observed tidal oscillations during a spring tide period. The first experiment includes the full model physics (as described in Sect. 4 and in the study of SWBBF). In the second experiment the same code is used, but the dynamics are switched off, that is, the sea level is horizontal and taken in the wet points as equal to the sea level corresponding to the mean forcing signal at the open boundary. The computations in the second experiment are, in fact, hypsometric computations of the time evolution of the volume of the tidal basins and could, in fact, be done without GETM. We have chosen to use the model in order to eliminate any differences which could arise from different coding.

According to the definitions in Section 2, the second experiment describes the first-order physical response and it will serve further as the reference response with which we compare the tidal response simulated with the model with active dynamics. In Fig. 14a the volumes of

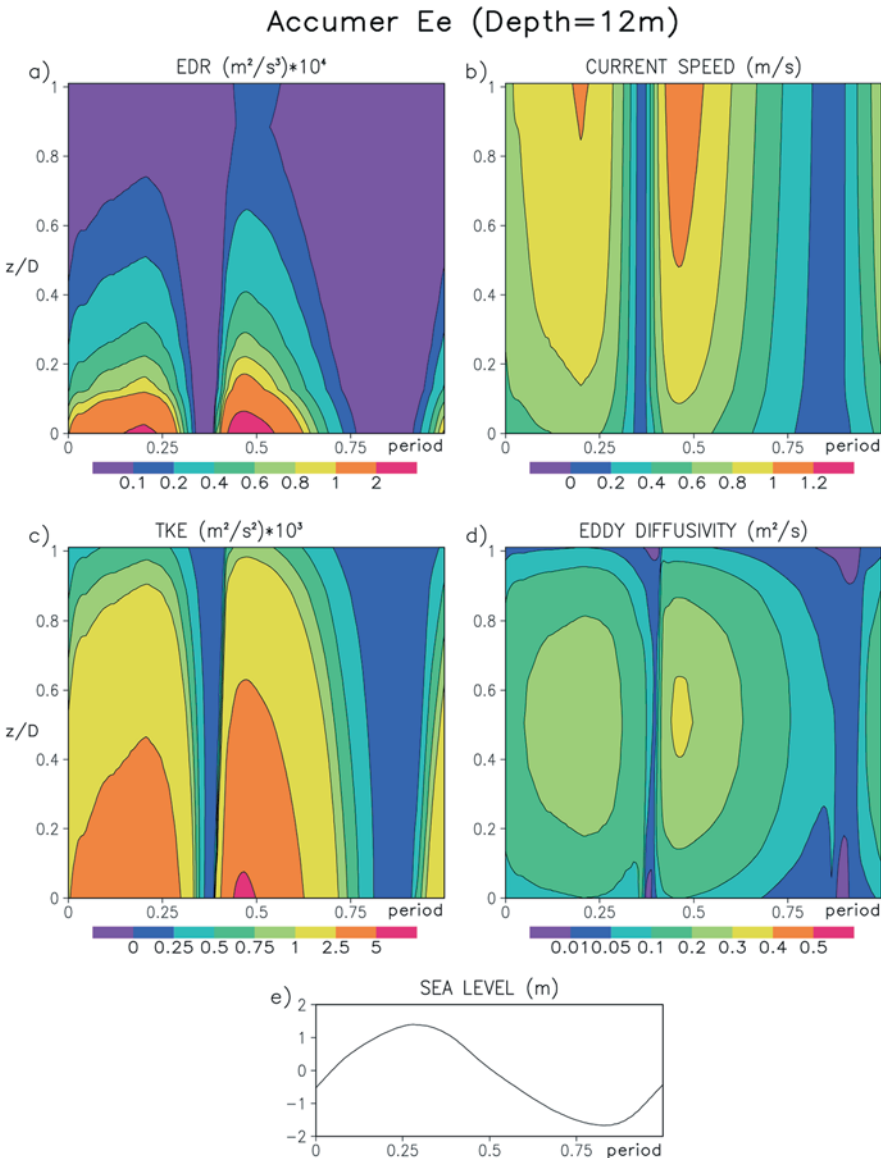

Fig. 13 Time versus depth plots during spring tide in the Accumer Ee. **a** The eddy dissipation rate (EDR), **b** the magnitude of velocity, **c** the turbulent kinetic energy (TKE) and **d** the coefficient of vertical turbulent exchange. The bottom plot **e** gives the sea level at the open boundary at the same latitude and for the same period as **a**–**d**

the tidal basins of the Islands Spiekeroog and Langeoog are shown. Figure 14b gives the volume changes. According to SWBBF, these changes approximately equal the water flux between intertidal basins and the ocean because the water flux between neighbouring basins is small compared to the transport through the inlets. The overall correlation between the two sets of curves demonstrates that simple volumetric computations give a first-order agreement with the case of active physics. However, as seen from Fig. 14c, which displays the difference between the volume changes in the two runs, there are periods when the inconsistency in the transport estimates from volumetric calculations reaches values which are comparable to the maximum transports. This actually gives an overall measure for the contribution of the higher-order dynamical controls. This contribution is strongest during the period of transition between maximum flood and maximum ebb conditions. This is the shorter phase of the tidal cycle and, as seen from Fig. 14b, the case of full physics is lagged compared to the case with only low-order dynamics included. The difference between the two results is an indication of the role of friction and non-linearity in the tidal system and could, at least partially, explain the scatter of the data in Fig. 10. The above conclusions are coherent with the patterns of sea-level anomaly in Fig. 11, which show very large gradients in the straits and deep channels during this part of the tidal period.

At this point it appears necessary to substantiate the considerations about the dominating dynamical balances given in Section 2.4. The best way to do this would be to use data from observations and to compare them with results from theoretical models (e.g., based on Eqs. 1–3). An alternative solution would suggest considering the data from numerical simulations as "real" data. Their comparison with the results from idealized models could help identify the dominating dynamical balances in the model, and perhaps in the real world. The

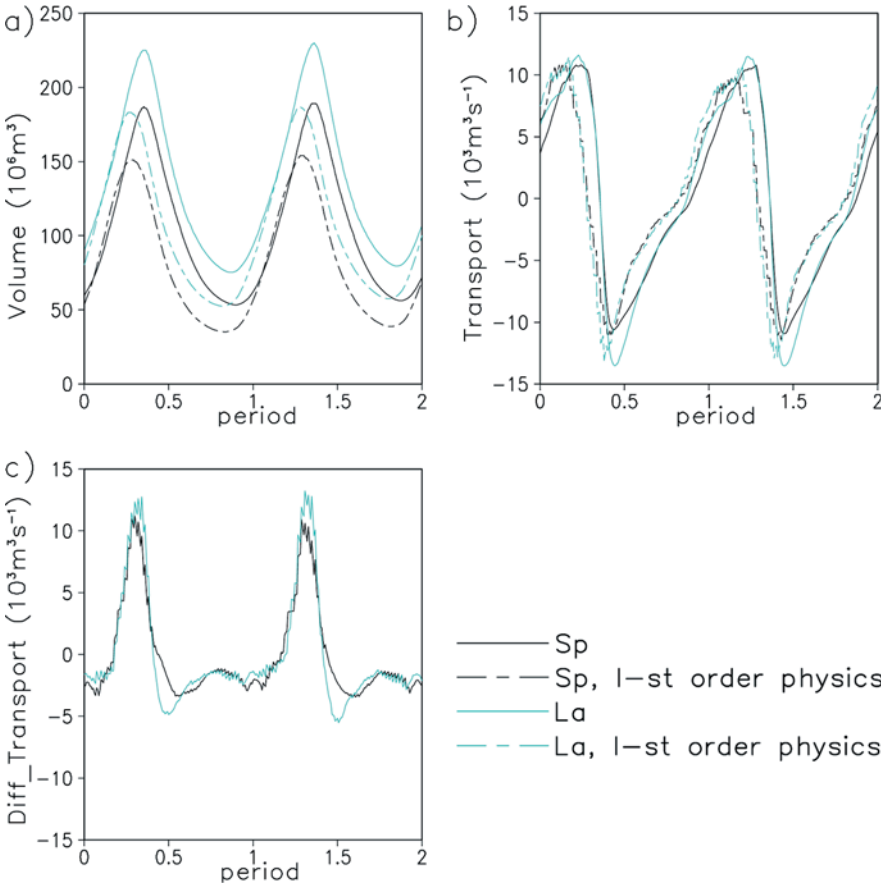

Fig. 14 Temporal variability of water volume **a**, its time rate of change **b** and the contribution of physical processes as seen in the difference between the time rate of change of volumes calculated in the case of active dynamics and first-order physics **c**

advantage of such an approach is that results from idealized models are clear and easy to understand.

We have chosen the following parameters for the system of Eqs. (1–3): $L_c = 4$ km, $h_c = 10$ m, $A_b^0 = 2.8 \times 10^7$ m^2, $A_c = h_c \times W = 2 \times 10^4$ m^2, where W is the width of inlet, $z_s = 2$ m, $a = 1.7$ m. The friction coefficient in Eq. (1) is described as

$$\gamma = \frac{gn^2}{h_c^{4/3}} \quad , \tag{39}$$

and we take for the standard value of Mannings coefficient $n_{\text{standard}} = 0.027$ m$^{-1/3}$s (see also Bruun 1978). We integrate Eqs. (1–3) under the following conditions: (1) low friction $n = \frac{1}{5} n_{\text{standard}}$, (2) standard friction $n = n_{\text{standard}}$, and (3) enhanced friction $n = 5 \times n_{\text{standard}}$. The results from the idealized model are shown in Figs. 15–17 for these three cases.

The friction in the low-friction case is too small to suppress the pumping mode (period ~ 1 h for the above set of parameters) and the corresponding oscillations are not negligible (Fig. 15). The frequency of these oscillations is not constant during the whole period (it increases when water level approaches minimum), which is a consequence of the time-variable geometry of the basin see Eq. 13. When $A_b = \text{const}$ (not shown here) these oscillations have a constant period. It is noteworthy that the amplitude of the short-periodic oscillations increases at the time of low water.

The red curve in Fig. 15b represents the transport computed in the case when $\zeta = \zeta_0$ in Eq. (37). This curve displays the same course as the theoretical curve in Fig. 6. The black transport curve on the same graph gives the response of the idealized model (Eqs. 1–3). This curve follows the general path of the red curve, the latter accounting for the simplest (first-order) balance in the model.

The bottom part of Fig. 15 displays the difference between the transport calculated by the idealized model and the transport corresponding to the lowest-order physical balance. Obviously, this differential transport measures the contribution of higher-order physics which, in this case, is dominated by the Helmholtz oscillations.

If we increase the friction coefficient by 25 times (a fivefold increase of n), we obtain its standard value, which is strong enough to suppress the Helmholtz mode. In this case (Fig. 16), the contribution of higher-order physics is small, as demonstrated by the fact that the black and red lines almost coincide. The transport reveals a similar course to what has been observed (Fig. 9) and simulated (Fig. 14). Obviously, the real dynamical system in the Wadden Sea tends to develop such balances, under which the first-order physical effects dominate the whole dynamical system. This is an illustration of the results from the assumptions in Section 2.4 which led us to the formulation of the first-order

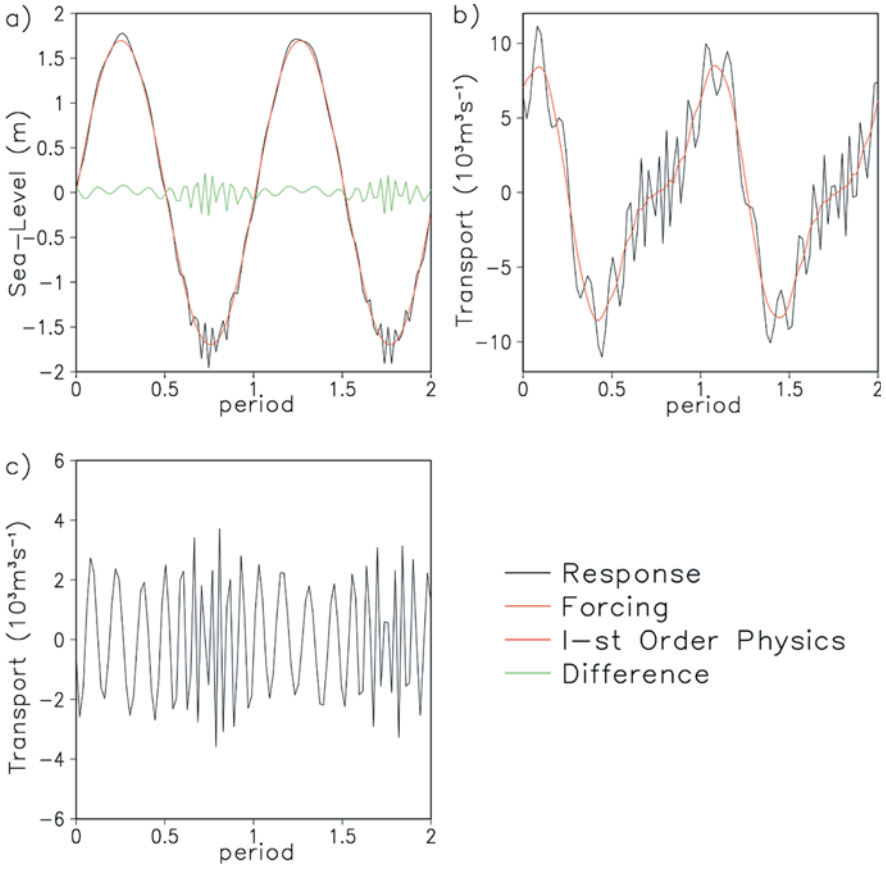

Fig. 15 Temporal variability of sea level **a** and transport **b** computed from the idealized model represented by Eq. (1) and Eq. (3) in the case of low friction. The basin area increases linearly with decreasing depth. See legend for line convention. The *red line* is used in **a** to denote the sea level in the open sea (ζ_0, that is, the forcing), while in **b** it represents the transport computed in the case when in Eq. (37) we take $\zeta = \zeta_0$. **c** Difference between the transports plotted in **b**

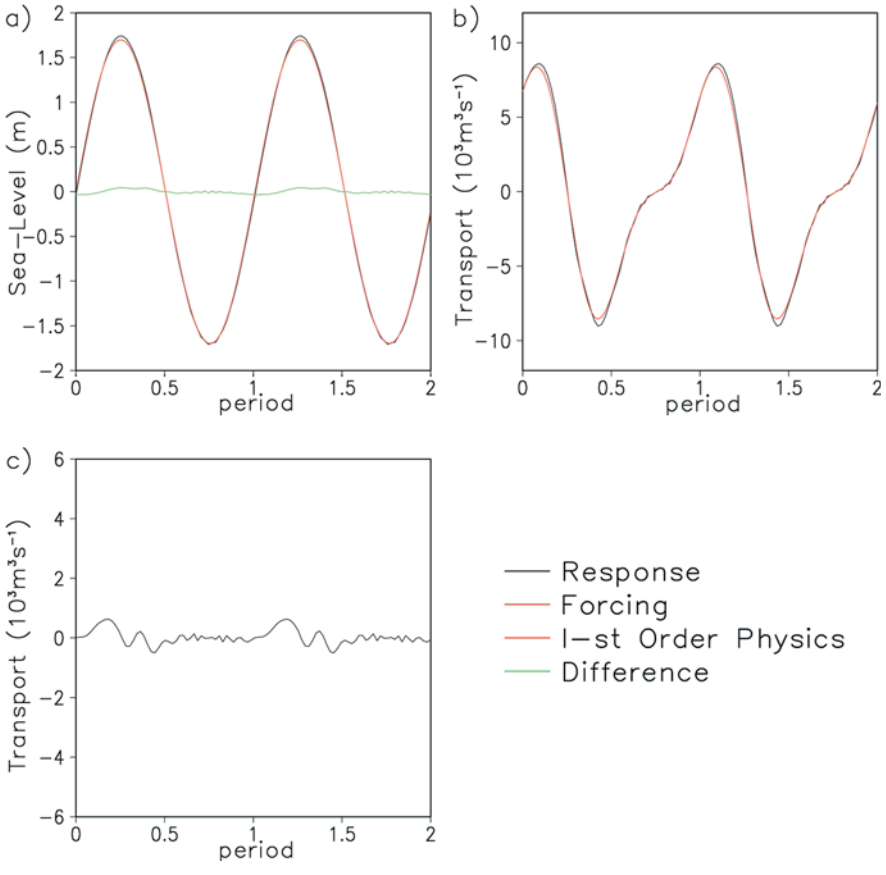

Fig. 16a–c As in Fig. 15 but for the case of standard friction

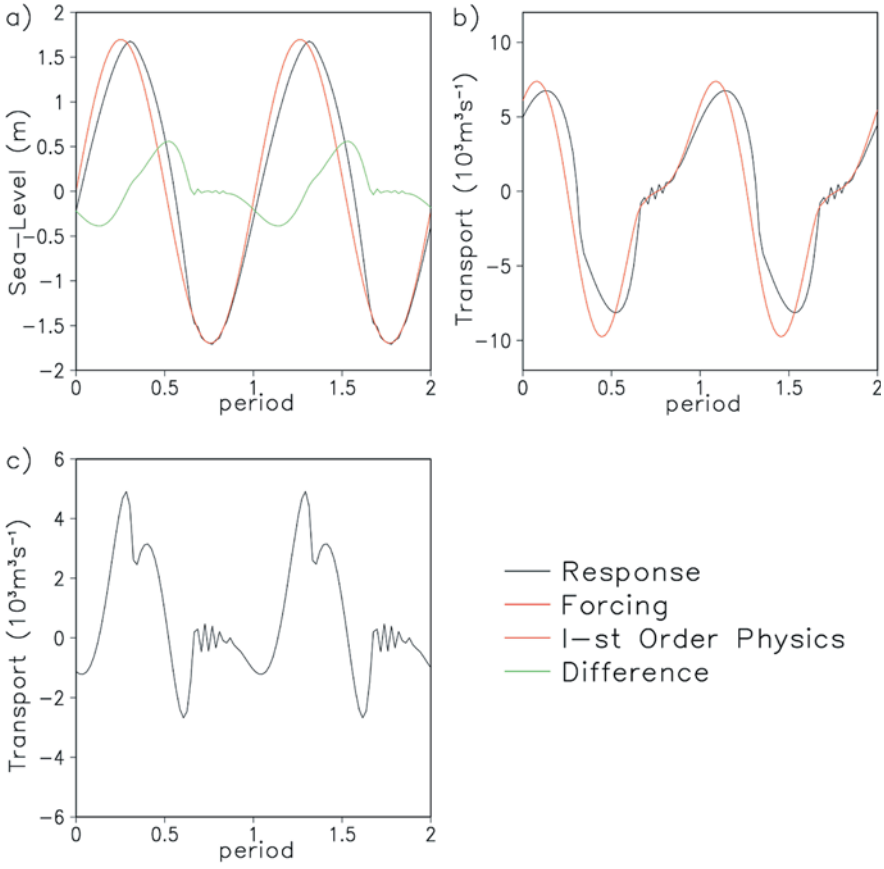

Fig. 17a–c As in Fig. 15 but for the case of enhanced friction

physical balance. We admit that this balance can be violated in some estuaries, as has been shown by Maas and Doelman (2002).

If we further increase n five times we again increase the contribution of the higher-order effects. However, in this case Helmholtz oscillations are suppressed by the high friction. One interesting result in Fig. 17a is that the response (as seen in the sea level) is lagged compared to the forcing at high water. The lag tends to zero at low water. This result is due to the linear increase of the basin area with the increasing depth. Our computations in the case $A_b = \text{const}$ (not shown here) demonstrate that the lag is equal at low and high water. In this context we recall that similar behaviour of the tidal response has been found by Friedrichs and Madsen (1992) in their theoretical analysis of frictionally dominated embayments.

The difference between the curves in Fig. 17b, giving the contribution of higher-order physics (Fig. 17c), reveals some features common with Fig. 14c. In particular, the main maximum (at about 0.3 T) and minimum (at about 0.6 T) appear on both figures. However, the small minimum just after the peak in Fig. 17c does not appear in Fig. 14c. Obviously, the idealized model captures some of the transport characteristics simulated in the three-dimensional model, which are associated with the higher-order physics, but not all of them.

One of the reasons why the results of idealized and realistic models differ could be due to different parameterizations. To check this hypothesis we substitute the friction term in Eq. (1) by a linear term and express the linear friction coefficient by Eq. (26), where $n = 5\times\, n_{\text{standard}}$ and $|u_{\text{mean}}| = 0.4\ \text{ms}^{-1}$ (see also Eq. 33). Figure 18c demonstrates that the theoretical curve is much closer to the one simulated in the 3-D model (Fig. 14c). This is an indication that the higher-order physics is better captured in this case than in the case with non-linear friction. This result becomes clear if we take into consideration that the dissipation in the model occurs not only in the straits (SWBBF) but also on the flats and in the tidal channels. Due to this, the friction in the straits is not so vigorous and better matches the linear parameterization in the latter case. It is clear now that the secondary maximum in the differential transport in Fig. 17c is a consequence of the non-linear friction. Another demonstration of the usefulness of idealistic models is the comparison between the curves corresponding to the basins of Langeoog and Spiekeroog (Fig. 14). In the basin of Spikeroog the absolute minimum is shallower and delayed in comparison to the case of Langeoog basin, which also indicates that higher-order physics does not contribute equally to the dynamics of the two basins.

6 Conclusions

The availability of an adequate numerical model and appropriate observational data ensured the calibration

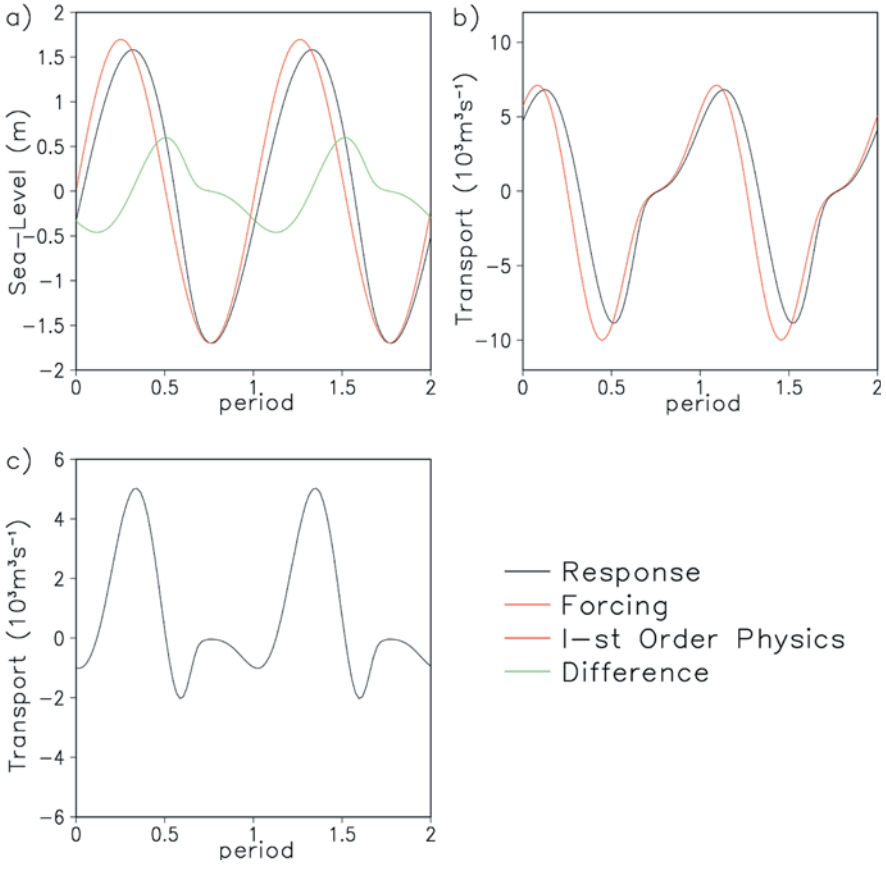

Fig. 18a–c As in Fig. 15 but for the case of linear friction

of the model and the realism of our simulations. This helped us to explore the possible errors when estimating the exchanges between tidal basins and the North Sea using simple concepts. The simulations analyzed here show a quite good agreement with the observations mainly because of the implementation of drying and flooding of intertidal flats. This is extremely important because the depth in the tidal basins is comparable to the tidal range. In this case the permanent water storage in these basins is smaller than the tidal prism; the export and import of waters through the inlets have different characteristic times at low and high water. This leads to the establishment of a non-linear response of the tidal basins where the major aspect is the much shorter transition from maximum flood to maximum ebb currents. Such response characteristics are found in other similar basins (Boon and Byrne 1981) and theoretical models (Friedrichs and Madsen 1992). They indicate that higher harmonics are created in tidal basins with variable depth. Our simulations reproduce this fundamental transformation of the signals which is controlled by the bottom slope in the areas prone to drying and flooding.

It is noteworthy that the transport curves obtained theoretically support those computed using the simple hypsometric approach, as well as those based on observations. However, they contradict the view presented by Postma (1982) about the temporal asymmetries (see his Fig. 36). We recall that in many other publications (e.g., Groen 1967) the type of asymmetry used as a physical background to explain the morphodynamics in tidal basins is "shorter-rising", that is the inverse to that in Fig. 6, the latter being "shorter-falling". However, it is the shorter-falling asymmetry which provides the basic signal in the response of the East Frisian tidal basins, as we demonstrated theoretically, from observations, as well as from model simulations. Obviously, any qualitative speculations about the transport of suspended particulate matter have to be made carefully, accounting for the realistic asymmetries which dominate the transports in the Wadden Sea, as well as the regime of turbulence. These issues will be addressed in a later publication. Here we only recall that from the analysis carried out in the paper by SWBBF it became clear that the specific distribution of turbulent kinetic energy, which is actually quite complicated in both time and space, is of crucial importance when addressing the predominating transport of sediments in the coastal zone.

The agreement between the independent estimates of the water exchange between the tidal basins and the open ocean gives good perspectives in reconstructing transports using simplified approaches and data, which are not collected over the entire basin. However, this agreement is not perfect and the differences between different estimates reflect the fact that the volumetric calculations based on sea-level measurements in one location only are not fully representative for the

exchanges between the tidal basins and the ocean. One important result of this study is that it enables us to objectively estimate the errors in the transport estimates, focusing on the difference between true transport and that explained by idealized models or hypsometric calculations only. This is achieved by formulating and testing concepts about the contribution of dynamics of increasing order. These concepts make the analysis of tidal responses clear, and allow a deeper understanding of the interplay between dynamics of different order.

The combination between data and modelling could lead to further improvement of estimates, and presents a challenging task when developing techniques for monitoring and data assimilation.

Acknowledgements We are indebted to S. Dick for providing the data from the operational model of BSH and to H. Burchard and K. Bolding for making GETM available to us. The comments of L. Maas on the theoretical part of paper are highly appreciated.

References

Boon JD III, Byrne RJ (1981) On the basin hypsometry and the morphodynamic response of coastal inlet systems. Mar Geol 40: 27–48

Bruun P (1978) Stability of tidal inlets. Theory and engineering. Developments in geotechnical engineering 23, Elsevier, Amsterdam, 506 pp

Burchard H, Bolding K (2002) GETM – a general estuarine transport model. Scientific documentation, no EUR 20253 EN, European Commission, printed in Italy, 157 pp

Dick SK, Eckhard K, Müller-Navarra SH, Klein H, Komo H (2001) The operational circulation model of BSH (BSHcmod) – model description and validation. Berichte des BSH: 29, 49 pp

Dick S, Schönfeld W (1996) Water transport and mixing in the North-Friesian Wadden Sea. Results of numerical investigations. Dt Hydrogr Zeitschrift 48: 27–48

Dick SK, Sötje K (1990) Ein operationelles Ölausbreitungsmodell für die deutsche Bucht. Dt Hydrogr Z, Ergänzungsheft Reihe (A) 16: 243–254

Doelman A, Koendernik AF, Maas LRM (2002) Quasi-periodically forced non-linear Helmholtz oscillators. Physica (D) 164: 1–27

Ferk U (1995) Folgen eines beschleunigten Meeresspiegelanstiegs für die Wattengebiete der niedersächsischen Nordseeküste. Die Küste. Archiv für Forschung und Technik an der Nord- und Ostsee. Heft 57: 135–156

Flemming BW, Davis RA (1994) Holocene evolution, morphodynamics and sedimentology of the Spiekeroog barrier island system (southern North Sea). Senkenbergiana Maritima 24: 117–155

Friedrichs CT, Aubrey DG (1988) Nonlinear tidal distortion in shallow well-mixed estuaries: a synthesis. Estuarine Coastal Shelf Sci 26: 521–545

Friedrichs CT, Madsen Os (1992) Nonlinear diffusion of the tidal signal in frictionally dominated embayments. J Geoph Res 97 C4: 5637–5650

Green T (1992) Liquid oscillations in a basin with varying surface area. Phys Fluids (A) 4: 630–632

Groen P (1967) On the residual transport of suspended matter by an alternating tidal current. Neth J Sea Res 3, 4: 564–574

Hayes M (1979) Barrier island morphology as a function of tidal and wave regime. In: Leatherman SP (ed) Barrier islands from the Gulf of St. Lawrence to the Gulf of Mexico. Academic Press, New York, pp 1–29

Hübner U, Backhaus JO (1997) Der küstennahe Gezeitenstrom im Gebiet der östlichen Ostfriesischen Inseln. Forschungszentrum Terramare, Ber 4: 65 pp

LeBlond PH (1978) On tidal propagation in shallow rivers. J Geophys Res 83 C9: 4717–4721

Lighthill J (1978) Waves in fluids. Cambridge University Press, Cambridge, 520 pp

Maas LRM (1997) On the nonlinear Helmholtz response of almost enclosed tidal basins with sloping bottoms. J Fluid Mech 349: 361–380

Maas LRM, Doelman A (2002) Chaotic tides. J Phys Oceanogr 32: 870–890

Postma H (1982) Hydrography of the Wadden sea: movements and properties of water and particulate matter. In: Postma (ed) Final report on Hydrography of the Wadden Sea Working Group – Report 2, Rotterdam, Balkema, 76 pp

Ridderinkhof H, Zimmermann JTF (1990) Mixing processes in a numerical model of the Western Dutch Wadden Sea. In: Cheng RT (ed) Coastal and estuarine studies. Springer, Berlin Heidelberg, New York, pp 194–209

Santamarina Cuneo P, Flemming B (2000) Quantifying the concentration and flux of suspended particulate matter through a tidal inlet of the East-Frisian Wadden Sea by acoustic Doppler current profiling. In: Flemming BW, Delafontaine MT, Liebezeit G (eds) Muddy coast dynamics and resource management. Elsevier Science, Amsterdam, pp 39–52

Schuttelaars HM, De Swart HE (2000) Multiple morphodynamic equilibria in tidal embayments. J Geoph Res 105 (C) 10: 24105–24118

Stanev EV, Wolff J-O, Burchard H, Bolding K, Flöser G (2003) On the circulation in the East-Frisian Wadden Sea: numerical modeling and data analysis. Ocean Dynamics, 53: 27–51